Journal of Biomechanics 92 (2019) 45–53

Contents lists available at ScienceDirect

Journal of Biomechanics

journal homepage: www.elsevier.com/locate/jbiomech
www.JBiomech.com

The effects of electromyography-assisted modelling in estimating musculotendon forces during gait in children with cerebral palsy

Kirsten Veerkamp [a,b,c,*], Wouter Schallig [a,e], Jaap Harlaar [a,f], Claudio Pizzolato [c,d], Christopher P. Carty [c,g], David G. Lloyd [c,d], Marjolein M. van der Krogt [a]

[a] Amsterdam UMC, Vrije Universiteit Amsterdam, Rehabilitation Medicine, Amsterdam Movement Sciences, de Boelelaan 1117, Amsterdam, the Netherlands
[b] Vrije Universiteit Amsterdam, Department of Behavioral and Movement Sciences, Amsterdam Movement Sciences, the Netherlands
[c] Gold Coast Centre for Orthopaedic Research, Engineering and Education (GCORE), Menzies Health Institute Queensland, Gold Coast, Australia
[d] School of Allied Health Sciences, Griffith University, Gold Coast, Australia
[e] Amsterdam UMC, Univ of Amsterdam, Radiology & Nuclear Medicine, Amsterdam Movement Sciences, Meibergdreef 9, Amsterdam, the Netherlands
[f] Delft University of Technology, Department of Biomechanical Engineering, Delft, the Netherlands
[g] Queensland Children's Motion Analysis Service, Children's Health Queensland Hospital and Health Service, Brisbane, Australia

ARTICLE INFO

Article history:
Accepted 16 May 2019

Keywords:
Biomechanics
Neuro-musculoskeletal modelling
OpenSim
Rehabilitation
Static optimization

ABSTRACT

Neuro-musculoskeletal modelling can provide insight into the aberrant muscle function during walking in those suffering cerebral palsy (CP). However, such modelling employs optimization to estimate muscle activation that may not account for disturbed motor control and muscle weakness in CP. This study evaluated different forms of neuro-musculoskeletal model personalization and optimization to estimate musculotendon forces during gait of nine children with CP (GMFCS I-II) and nine typically developing (TD) children. Data collection included 3D-kinematics, ground reaction forces, and electromyography (EMG) of eight lower limb muscles. Four different optimization methods estimated muscle activation and musculotendon forces of a scaled-generic musculoskeletal model for each child walking, i.e. (i) static optimization that minimized summed-excitation squared; (ii) static optimization with maximum isometric muscle forces scaled to body mass; (iii) an EMG-assisted approach using optimization to minimize summed-excitation squared while reducing tracking errors of experimental EMG-linear envelopes and joint moments; and (iv) EMG-assisted with musculotendon model parameters first personalized by calibration. Both static optimization approaches showed a relatively low model performance compared to EMG envelopes. EMG-assisted approaches performed much better, especially in CP, with only a minor mismatch in joint moments. Calibration did not affect model performance significantly, however it did affect musculotendon forces, especially in CP. A model more consistent with experimental measures is more likely to yield more physiologically representative results. Therefore, this study highlights the importance of calibrated EMG-assisted modelling when estimating musculotendon forces in TD children and even more so in children with CP.

1. Introduction

Cerebral palsy (CP) is one of the most common motor disorders among children with an incidence of 2–2.5 per 1000 live births (Cans, 2000). Common impairments in CP include hyper-reflexia, impaired selective motor control, contractures and muscle weakness (Graham et al., 2016). Both these neural and non-neural impairments often lead to problems with gait in people with CP. Many interventions target the muscles in order to improve gait performance. Neuro-musculoskeletal modelling can be a valuable tool by providing more insights in how individual muscles contribute to gait, for example by estimating muscle forces. However, given the countless number of potential neural solutions that can be employed to execute a single movement, a major challenge is to solve the redundancy problem (Crowninshield and Brand, 1981).

Static optimization is a commonly used mechanical approach to solve the redundancy problem, assuming, for example, minimization of the muscle activation squared (Michnik et al., 2009; Modenese et al., 2011; Steele et al., 2012; Wesseling et al., 2016). In order to achieve representative force estimates in children when using static optimization, it has been suggested that it is essential

* Corresponding author at: Amsterdam UMC, Vrije Universiteit Amsterdam, Rehabilitation Medicine, Amsterdam Movement Sciences, de Boelelaan 1117, Amsterdam, the Netherlands.
E-mail address: k.veerkamp@vumc.nl (K. Veerkamp).

https://doi.org/10.1016/j.jbiomech.2019.05.026
0021-9290/

to scale the maximum isometric forces (MIFs) of the musculotendon units of the model instead of using generic values based on healthy adults (Kainz et al., 2018; Van der Krogt et al., 2016). However, previous studies have not quantified model performance without and with MIF scaling. This personalization step may even be extra important in children with CP, who often have muscle weakness (Graham et al., 2016). Moreover, also after scaling MIF, the resulting muscle recruitment may not represent an individual's motor control. The assumption that all individuals employ similar neuromuscular strategies to perform a movement is in disagreement with experimental findings that show that for the same joint angles and joint moments EMG patterns vary between individuals (Lloyd and Buchanan, 2001), and in the same people EMG patterns (Buchanan and Lloyd, 1995; Milner and Cloutier, 1998) and motor unit recruitment (Tax et al., 1990) vary when the same movement is involved in a different task. A recent study by Trinler et al. (2018) indicated that activations estimated by static optimization did not agree well with measured EMG at different walking speeds in healthy individuals. Moreover, due to the aberrant motor control in children with CP, the use of a static optimization approach solely minimizing activation squared to solve the redundancy problem is likely to be even more problematic in this clinical population.

Subsequently, applying an EMG-assisted approach (Pizzolato et al., 2015; Sartori et al., 2014) to solve the neuromusculoskeletal model's muscle activation patterns may be required to generate more physiologically plausible estimates of muscle forces. In such an approach, recorded EMG signals provide first estimates of the muscle excitations, while static optimization both synthesizes excitations for muscles that do not have EMGs, and adjusts the EMG-derived excitations to account for errors associated with surface EMG (Farina and Negro, 2012; Sartori et al., 2014). Moreover, EMG can be used to calibrate musculotendon parameters of the model to individual properties (i.e. tendon slack length, optimal fiber length and MIF), by using an optimization procedure to best match experimental and estimated joint moments (Lloyd and Besier, 2003; Pizzolato et al., 2015; Sartori et al., 2012). Musculoskeletal model outputs have previously been shown to be very sensitive to changes in these parameters (Carbone et al., 2016; Out et al., 1996; Scovil and Ronsky, 2006; Xiao and Higginson, 2010). However, calibrated EMG-assisted approaches have not been applied in children, nor in CP.

This study evaluated the effects of different steps of personalization in estimating musculotendon forces in both typically developing (TD) children and children with CP. Four neuromusculoskeletal modelling methods with increasing levels of personalization were created. Model performance was assessed by comparing model predictions of experimental measures: joint moments and muscle EMG-linear envelopes. It was hypothesized that increasing the level of personalization increases model performance, especially when using an EMG-assisted approach instead of static optimization solely minimizing excitations squared. Furthermore, it was hypothesized that the use of an EMG-assisted approach results in a higher improvement of model performance in CP than in TD children.

2. Methods

2.1. Participants

Nine children with spastic CP (6 males, age = 11.4 ± 2.2 years, body mass = 40.6 ± 9.6 kg, height = 149.9 ± 11.8 cm) and nine TD children (6 males, age = 10.0 ± 2.2 years, body mass = 38.0 ± 9.4 kg, height = 148.3 ± 14.8 cm) participated in the study. CP participants were classified as level I (3 children) or II on the Gross Motor Function Classification System (Palisano et al., 1997). Eight CP participants were affected bilaterally (legs only) and one was affected unilaterally. Patients who had a relevant visual deficit, insufficient cognitive skills to follow simple instructions or significant comorbidities, or underwent orthopedic or neurosurgical surgery less than 1 year ago, were excluded from the study. Ethics approval was obtained from the local medical ethics committee and informed consent was provided by all parents and children of 12 years or older.

2.2. Data acquisition

Participants were affixed with 41 reflective markers (Fig. 1) of which the three-dimensional marker trajectories were captured at 100 Hz with a Vicon MX optoelectronic system (Vicon, Oxford, UK). A dual-belt treadmill in a projected virtual environment (Gait Real-time Analysis Interactive Lab (GRAIL) system, Motek BV, The Netherlands) was used, equipped with an R-MILL force platform (100 Hz) to measure ground reaction forces. Furthermore, muscle activity of eight muscles (specified in Table 1) on each leg was

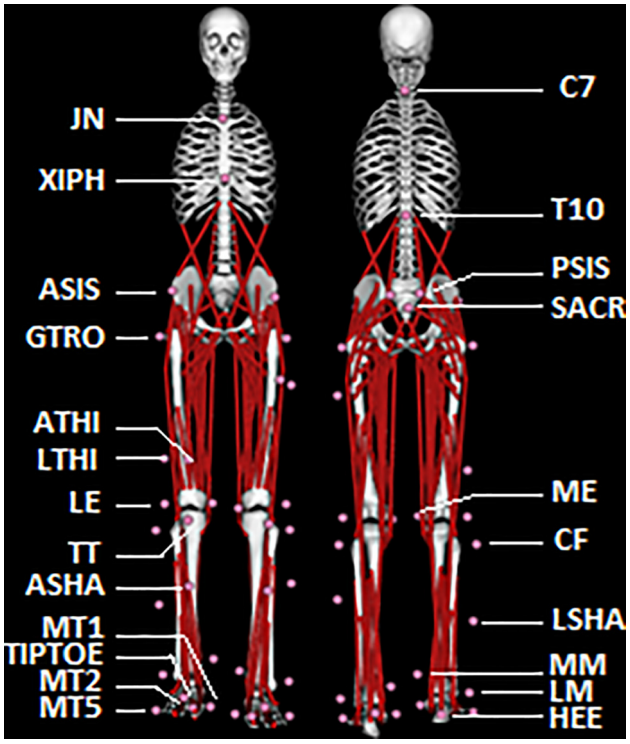

Fig. 1. An example of a scaled generic musculoskeletal model that was used, including the 41 markers (pink circles). (For interpretation of the references to colour in this figure legend, the reader is referred to the web version of this article.)

Table 1
Recorded EMG signals and innervated model musculotendon complexes.

Measured EMG	Innervated model musculotendon complexes
Gluteus medius	glut_med1, glut_med2, glut_med3, glut_min1, glut_min2, glut_min3
Rectus femoris	rect_fem
Vastus lateralis	vas_lat, vas_med, vas_int
Semitendinosus	semiten, semimem
Biceps femoris long head	bifemlh, bifemsh
Tibialis anterior	tib_ant
Gastrocnemius medius	med_gas, lat_gas
Soleus	soleus

Musculotendon complexes are named as in OpenSim.

measured (16-channel EMG Cometa Zero Wire, Italy). EMG electrodes were placed in accordance to SENIAM guidelines (Hermens et al., 1999). Each participant performed a familiarization trial at the GRAIL. Afterwards, a static trial (T-pose) was captured and followed by walking trials at four different, self-selected speeds (comfortable, slow, fast and fastest). Each participant walked on the GRAIL for at least 30 s at each walking speed.

2.3. Data processing

Kinematic and kinetic data were filtered with 6 Hz second order low pass Butterworth filters. All ground reaction force values equal to and less than 30 N were associated with measurement artefacts and therefore set to zero. EMG data were filtered with a recursive second order Butterworth bandpass filter between 30 and 300 Hz, full-wave rectified and subsequently filtered with a recursive second order Butterworth low pass filter of 6 Hz to obtain the EMG-linear envelopes. EMGs were normalized for the individuals' highest values measured during all walking trials.

Analysis was performed for the most affected leg of each child with CP, and for the right leg for each TD participant. For each participant, data (ground reaction forces, EMG and marker data) of four gait cycles at comfortable walking speed were selected for the neuro-musculoskeletal modelling analysis. One gait cycle at each of the four walking speeds was selected for calibration of the model (described later). 100 ms were added before and after the full gait cycles for further analysis to ensure continuity around initial contact.

2.4. Neuro-musculoskeletal models preparation

A generic scaled model of each participant was generated using the gait2392 model (Delp et al., 1990) in OpenSim (version 3.3, (Delp et al., 2007)). This 23-degree-of-freedom model consisted of 92 musculotendon units, representing 76 muscles in the lower extremities and torso. The model was modified by locking the subtalar joint. Using the OpenSim Scaling tool, the model's segments were linearly scaled by matching virtual markers of the generic OpenSim model to experimental markers measured during the static trial of the participant. Musculotendon parameters were scaled linearly according to the change in musculotendon length. Body mass was also scaled, while the segment masses were kept proportionally consistent. OpenSim inverse kinematics, inverse dynamics and muscle analysis tools were used to calculate joint angles, joint moments and musculotendon lengths and moment arms during gait.

Musculotendon forces were estimated using the Calibrated EMG-Informed Neuromusculoskeletal Modelling (CEINMS) OpenSim Toolbox (Pizzolato et al., 2015; Sartori et al., 2014), in which the following function was minimized:

$$F = \alpha E_{trackMOM} + \beta E_{sumEXC^2} + \gamma E_{trackEMG} \quad (1)$$

in which $E_{trackMOM}$ was the sum of squared differences between predicted and experimental joint moments; E_{sumEXC^2} was the sum of squared excitations for all musculotendon units; and $E_{trackEMG}$ represented the sum of the differences between the experimental excitations (i.e. EMG-linear envelopes) and the adjusted model excitations. α, β and γ were positive weighting factors of each component. Force-length, force-velocity, and tendon force-strain relationships were according to Thelen (2003). Activation dynamics were determined by a critically-damped, linear second-order differential system (Lloyd and Besier, 2003; Pizzolato et al., 2015).

Four different methods with increasing levels of personalization were used to estimate musculotendon forces. The first method used static optimization to estimate musculotendon forces. The sum of excitation squared was minimized, by setting $\alpha = 1$, $\beta = 1$ and $\gamma = 0$ in Eq. (1). In the second method the MIF of each musculotendon unit was scaled to body mass (m_{new}) of the participant, using Eq. (2) (Van der Krogt et al., 2016) before using static optimization.

$$MIF_{new} = MIF_{g2392} * \left(\frac{m_{new}}{m_{gait2392}}\right)^{\frac{2}{3}} \quad (2)$$

The third method used an EMG-assisted approach to estimate musculotendon forces, in which tracking of EMG excitations was implemented into the optimization procedure. Measured EMGs were used to drive the model's musculotendon units as specified in Table 1. In the EMG-assisted procedure, using Eq. (1), α and β were set to 1, and γ was tuned to a value ≥ 1 by balancing the tracking of both the experimental excitations and the joint moments, based on Sartori et al. (2014).

The fourth method used CEINMS calibration before using the EMG-assisted approach. Within this calibration, EMG-driven neuro-musculoskeletal modelling was used to calculated the joint moments of one gait cycle at each walking speed (Pizzolato et al., 2015; Sartori et al., 2014). The calibration adjusted musculotendon model parameters to minimize the error between the predicted EMG-driven joint moments and the inverse dynamics joint moments in these trials. The musculotendon parameters of the model were bounded, with tendon slack length and optimal fiber length of each musculotendon unit calibrated within ±5% of their initial value. Musculotendon units were divided into muscle groups based on function to calibrate their MIF, which was already scaled by Eq. (1). For each muscle group a strength coefficient was calibrated between 0.5 and 3.5, affecting the MIF of the musculotendon units within each muscle group.

2.5. Data analysis

Three outcomes of the different modelling methods were analyzed: the joint moments, the muscle excitations and the musculotendon forces. Model's estimates of joint moments and excitations were compared to experimental measures – i.e. inverse dynamics joint moments and EMG-linear envelopes, respectively – to assess model performance. As musculotendon forces could not be compared to experimental data, it was assumed that the most personalized model – with the calibrated musculotendon parameters and an EMG-assisted approach – resulted in the physiologically most correct estimates of musculotendon forces (Gerus et al., 2013; Hoang et al., 2018, 2019; Serrancolí et al., 2016). Hence, for all 43 musculotendon units in the analyzed leg the forces estimated by the calibrated EMG-assisted model were compared to the forces estimated by the other models to assess how the different personalization steps affected the forces. For all three outcomes the agreements were quantified by the coefficient of determination (R^2) and root mean squares error (RMSE), using a custom program in Matlab 2016a (The MathWorks Inc., MA).

2.6. Statistics

A mixed ANOVA was performed to compare each of the outcome measures assessing model performance (the R^2 and RMSE of both joints moments and excitations) between methods within groups. Also the R^2 and RMSE of the agreement of the musculotendon forces with the EMG-assisted calibrated model were compared by a mixed ANOVA. Significance level set at $\alpha = 0.05$. If Mauchly's test of sphericity was significant, indicating that the assumption of sphericity was violated, depending on the Epsilon of Greenhouse-Geisser either the Greenhouse-Geisser correction (if epsilon < 0.75) or the Huyn-Feldt correction (if epsilon ≥ 0.75)

was used. Post-hoc tests with repeated contrasts and Bonferroni corrections were performed to further analyze significant main and interaction effects. All statistical analyses were performed using IBM SPSS Statistics (version 20, SPSS INC., Chicago, IL, USA).

3. Results

3.1. Joint moments

All modelling methods tracked joint moments well in TD and CP groups (Fig. 2), demonstrated by high R^2 values ($\geq$0.98) and low RMSE values (<0.036 Nm/kg; Table 2 and Fig. 3A and B). All methods exhibited mainly small deviations in the knee joint moment, at around 60% of the gait cycle for both CP and TD subjects. Appendix A gives an overview of R^2 and RMSE values for each individual joint moment in both groups.

The R^2 between the models' and inverse dynamics joint moments (Fig. 3A) revealed no significant main effect of group ($p = 0.50$), nor a significant main effect of modelling method ($p = 0.46$). The R^2 of moments did show a significant interaction effect between group and modelling method ($p = 0.020$). Between method 2 (static optimization with scaled MIF) and method 3 (EMG-assisted) the moments' R^2 increased for CP but decreased for TD ($p = 0.024$). The R^2 decreased for CP but increased for TD when calibrating the musculotendon units ($p = 0.006$). However, all differences were very small (<0.015).

Joint moments' RMSEs (Fig. 3B) were significantly higher for TD than for CP ($p = 0.029$). Modelling method did have a significant main effect ($p < 0.001$), in which the moments' RMSE was significantly increased when scaling the MIF ($p < 0.001$) and when changing to an EMG-assisted approach ($p = 0.044$). There was a significant interaction effect between group and model ($p = 0.0032$). When scaling the MIF, the increase was higher for CP than for TD ($p = 0.014$), the RMSE increased for TD and decreased for CP when using an EMG-assisted approach ($p = 0.010$), while it decreased for TD but increased for CP after calibration ($p = 0.016$). But importantly, again, the differences between methods were very small (<0.018).

3.2. Muscle excitations

The static optimization estimated excitations were clearly distinguishable from the EMG-linear envelopes for each musculotendon unit in both groups (Fig. 4). Differences were visible both in pattern and amplitude, mainly in the hamstrings (semiten, semimem, bifemlh and bifemsh), gastrocnemii (med gas and lat gas) and rectus femoris (rect fem). The matching with EMG excitations was substantially better when using an EMG-assisted approach. Appendix A gives an overview of R^2 and RMSE values for individual musculotendon units for both groups.

The R^2 between the models' muscle excitations and EMG-linear envelopes (Fig. 3C and Table 2) was significantly higher for CP than for TD ($p = 0.013$). There was a significant main effect for modelling method ($p < 0.001$) in which the R^2 significantly increased when scaling the MIF ($p < 0.001$) and when using an EMG-assisted approach ($p < 0.001$). Also, there was a significant interaction effect between group and modelling method for activations' R^2 ($p = 0.023$), increasing more for CP than for TD when using an EMG-assisted method ($p = 0.013$).

The RMSE of the modelled excitations compared to the EMG-linear envelopes (Fig. 3D and Table 2) did not show a significant main effect of group ($p = 0.36$). There was a significant main effect of modelling method ($p < 0.001$), in which the RMSE decreased significantly when using an EMG-assisted approach ($p < 0.001$). A significant interaction effect ($p = 0.013$) indicated that scaling the MIF increased the RMSE for TD children, but reduced the RMSE for CP

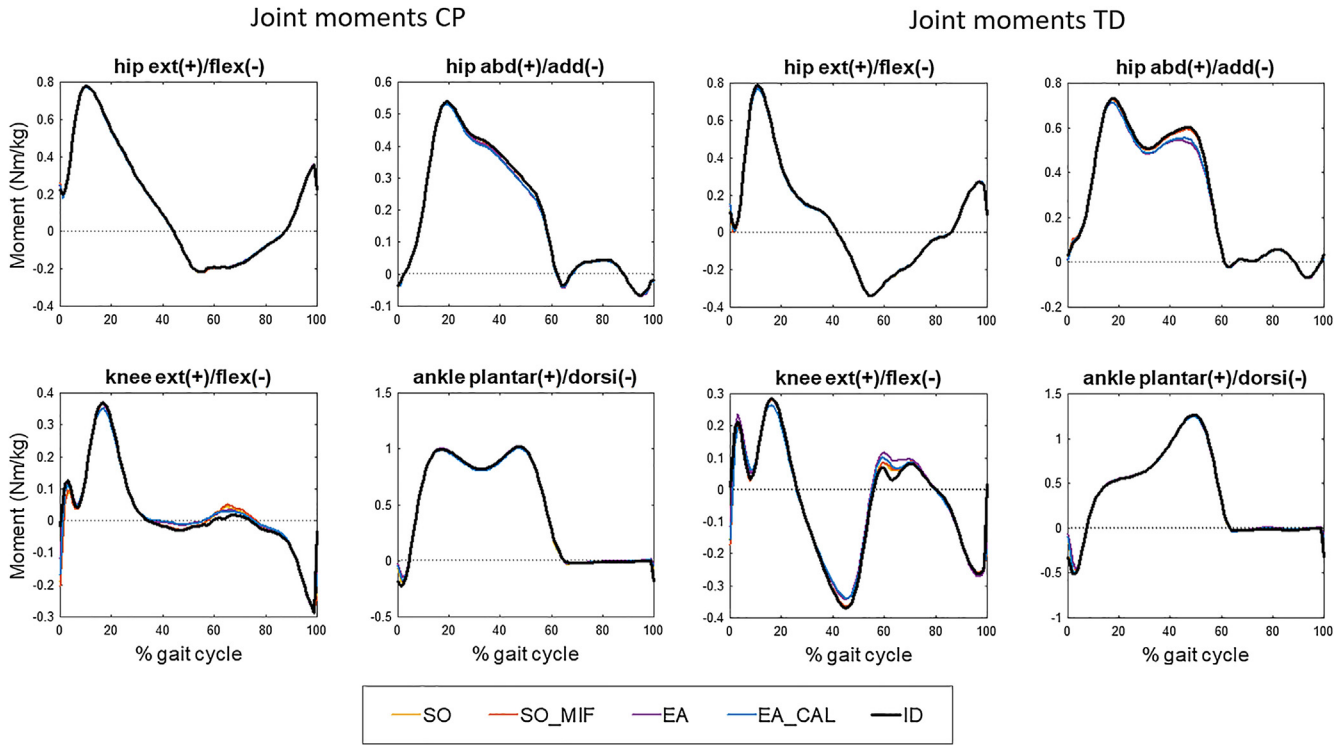

Fig. 2. Mean joint moments for both CP (left) and TD (right) children for the hip (extension/flexion and abduction/adduction), knee (extension/flexion) and ankle (plantarflexion/dorsiflexion). Generally, all models achieved good tracking of the inverse dynamics (ID) moments. SO: static optimization with generic maximum isometric forces (MIFs). SO_MIF: static optimization with MIFs scaled to body mass. EA: EMG-assisted approach. EA_CAL: EMG-assisted approach with calibrated musculotendon parameters.

Table 2
Agreement of model joint moments and excitations with the experimental measures (mean ± SD).

		SO		SO_MIF		EA		EA_CAL		Significance		
		CP	TD	CP	TD	CP	TD	CP	TD	Group	Method	Group*method
Joint moments	R^2	0.99 ± 0.012	0.99 ± 0.0082	0.98 ± 0.015	0.99 ± 0.013	0.99 ± 0.0058	0.98 ± 0.021	0.99 ± 0.0059	0.98 ± 0.020	0.50	0.46	**0.020**
	RMSE (Nm/kg)	0.018 ± 0.0062	0.020 ± 0.0082	0.020 ± 0.0077	0.026 ± 0.011	0.019 ± 0.0083	0.036 ± 0.011	0.020 ± 0.0067	0.032 ± 0.011	**0.029**	**<0.001**	**0.0032**
Excitations	R^2	0.16 ± 0.030	0.15 ± 0.032	0.21 ± 0.029	0.19 ± 0.040	0.58 ± 0.11	0.41 ± 0.093	0.55 ± 0.14	0.44 ± 0.11	**0.013**	**<0.001**	**0.023**
	RMSE	0.21 ± 0.055	0.16 ± 0.026	0.20 ± 0.045	0.18 ± 0.025	0.098 ± 0.027	0.11 ± 0.014	0.11 ± 0.027	0.11 ± 0.016	0.36	**<0.001**	**0.013**

Bold indicates significant at p<0.05.

(p = 0.003). The use of an EMG-assisted approach led to a higher decrease in RMSEs in CP than in TD (p = 0.027).

3.3. Musculotendon forces

Fig. 5 shows the agreement between the musculotendon forces estimated by the EMG-assisted calibrated model and the other models, quantified by the R^2 (left) and RMSE (right). The R^2 only showed a significant main effect of model (p < 0.001), in which both static optimization approaches showed a significantly lower R^2 than the EMG-assisted method (p < 0.001). Thus, using an EMG-assisted approach instead of static optimization substantially affected the pattern of the musculotendon forces. The gastrocnemii and rectus femoris showed clear differences in pattern over the gait cycle in CP, the gluteus minimus and first component of the gluteus maximus in TD (Appendix B). Over all methods, the RMSE was significantly higher for CP (p = 0.007). There was a significant main effect of model, in which scaling the maximum isometric forces significantly reduced the RMSE compared to the calibrated EMG-assisted model (p < 0.001). A significant interaction effect (p = 0.009) indicated that using an EMG-assisted approach instead of static optimization reduced the RMSE compared to the calibrated EMG-assisted model in TD children, while it increased in CP. Hence, calibrating the musculotendon parameters affected the amplitude of the forces more for CP than for TD. This was especially visible in the biceps femoris, rectus femoris and gastrocnemii (Appendix B).

4. Discussion

This study evaluated the effects of different steps of personalization in neuro-musculoskeletal modelling in estimating musculotendon forces in both TD and CP children. As expected, a significant and clinically meaningful improvement in tracking of experimental EMG excitations, with no significant loss in tracking accuracy of inverse dynamics joint moments was shown for an EMG-assisted approach compared to static optimization methods. Conforming our hypothesis, both the RMSE and the R^2 of the agreement of model excitations with EMG-linear envelopes showed a significant interaction effect, in which the improvement when using an EMG-assisted approach was higher for CP than for TD. As a model more consistent with experimental measures is more likely to yield more physiologically representative outcomes, these results highlight the importance of guiding model solutions with experimental measures of neuromuscular control when estimating musculotendon forces, especially in CP. Furthermore, calibration of musculotendon parameters substantially affected estimated musculotendon forces in children with CP, indicating that a calibrated EMG-assisted method responds better to differences between CP and TD children.

Regarding estimated excitation patterns, overall, static optimization model performance was weak for both groups, showing a relatively low agreement with EMG-linear envelopes. This still occurred even when the MIF was scaled to a more realistic value. The static optimization solutions did not account for the individual differences in muscle activations (Buchanan and Shreeve, 1996), which could explain this finding. Static optimization has been one of the most commonly used methods to estimate musculotendon forces (Michnik et al., 2009; Modenese et al., 2011; Steele et al., 2012; Wesseling et al., 2016), as it is an accessible tool, for example implemented in OpenSim. However, when comparing the activations resulting from this static optimization tool to EMG linear envelopes, also some clear differences were visible for some muscles in both TD children and children with CP (Steele et al., 2012). Another strategy often used to obtain muscle

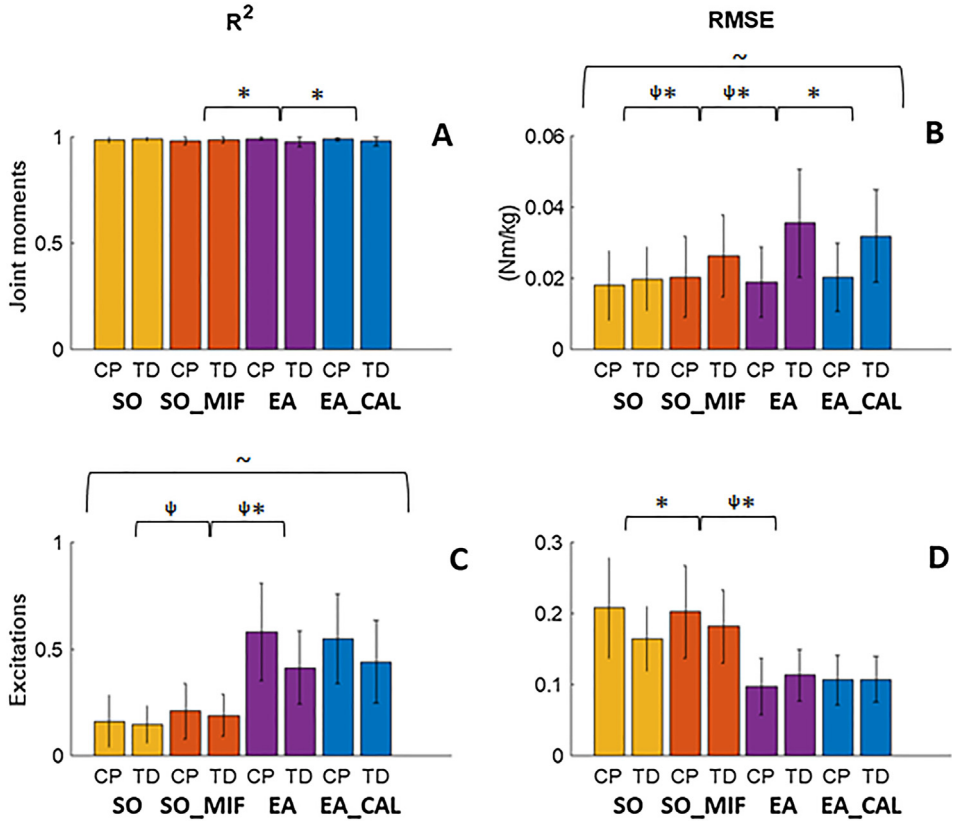

Fig. 3. A and B show the agreement of the model joint moments with the inverse dynamics joint moments, which was generally high for each modelling approach, as indicated by a high R^2 and a low RMSE. C and D show the agreement between the model activations and the EMG activations. R^2 increased substantially when using an EMG-assisted (EA and EA_CAL) compared to static optimization (SO and SO_MIF), while the RMSE decreased. ψ indicates a significant main effect between methods; ~ indicates a significant main effect of group; * indicates a significant interaction effect between methods.

activations is computed muscle control (e.g. Hamner et al., 2010; Liu et al., 2008; Steele et al., 2010; Trinler et al., 2018; Van der Krogt et al., 2012), which is also a tool in OpenSim (Thelen et al., 2003; Thelen and Anderson, 2006). This procedure might improve model performance compared to static optimization, since it adds feedback and feedforward control, implementing time-dependency of the solution. However, studies using computed muscle control also showed clear discrepancies between computed activations and EMG solutions in healthy individuals (Hamner et al., 2010; Liu et al., 2008; Steele et al., 2010; Trinler et al., 2018; Van der Krogt et al., 2012). Hence, the weight of available evidence suggests that the commonly used optimization approaches which do not implement recorded excitations might not be appropriate in estimating musculotendon forces in healthy individuals, let alone individuals with neuromuscular impairments.

The present study showed that EMG-assisted modelling provided a more physiologically realistic solution for the redundancy problem. Compared to static optimization approaches, EMG-assisted methods improved agreement with experimental EMG. This was to be expected, as implementing EMG into the optimization procedure will obviously increase agreement with experimental excitations. Importantly, however, such an EMG constrained optimization did not compromise on relevant agreement with experimental joint moments. Moreover, it was found that the increase in model performance when using an EMG-assisted approach was especially relevant in CP, indicating that optimizing by solely minimizing muscle excitations squared may particularly not be appropriate for this group. Static optimization does not account for co-contraction, one of the features of the impaired selective muscle control in CP, as also indicated by the higher RMSE between the estimated excitations and the EMG-linear envelopes for the static optimization methods compared to TD children. Interestingly, the R^2 of the excitations was substantially higher for CP than for TD. Possibly, the aberrant gait pattern in children with CP results in less possible solutions for the muscle activation patterns, leading to a higher agreement with the EMG-linear envelope patterns than for TD, also when solely minimizing excitation squared.

Calibrating the model did not result in a significant improvement in agreement with experimental data in both groups. However, calibration did affect the resulting musculotendon force estimates, especially in amplitude in children with CP. Previous studies showed that calibration is an essential step in obtaining accurate results in estimating joint contact forces, when compared to in vivo measured values (Gerus et al., 2013; Serrancolí et al., 2016). To improve the tuning of the model to the individual, additional optimization criteria might be essential, such as minimization of the joint contact forces, which further improved the physiological feasibility of the estimated joint contact forces in previous studies (Gerus et al., 2013; Hoang et al., 2018, 2019; Serrancolí et al., 2016). It would be advised to further investigate whether the changed parameters after calibration get closer to realistic values. Generally, the strength coefficients of most muscle groups were reduced to close to the lowest bound (0.5) after calibration, resulting in a weaker model, even after MIF was already scaled to body mass. This finding might also have been influenced by the EMG normalization, which was conducted using the maximum value across walking speeds. However, not all muscles will have been maximally activated at some point during walking, even

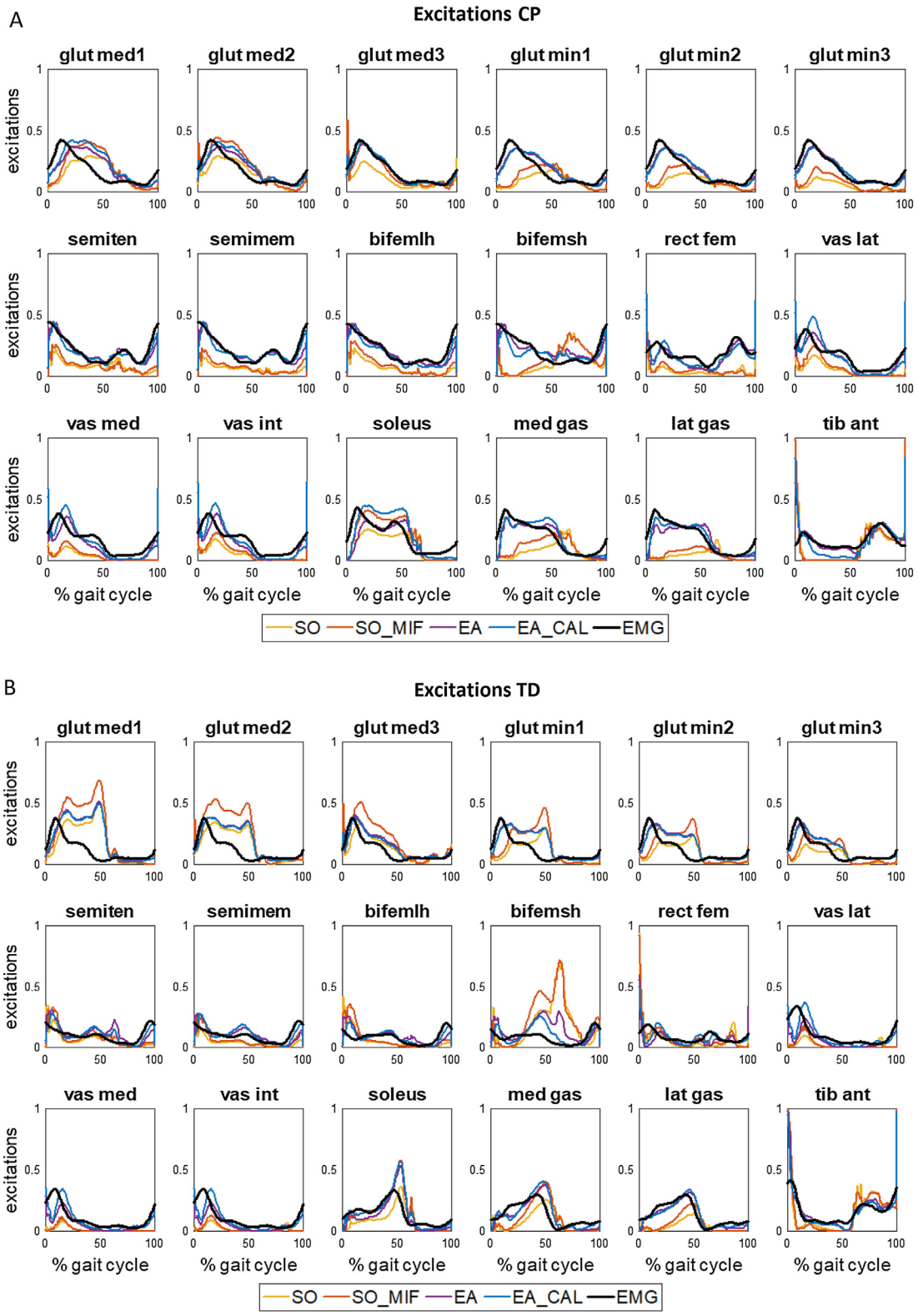

Fig. 4. The EMG linear envelopes and the excitations of each modelling approach for CP (A) and for TD (B). The static optimization approaches (SO and SO_MIF) showed generally a weak agreement with EMG excitations, both in amplitude and pattern. Using an EMG-assisted (EA) approach obviously improved the agreement with EMG excitations substantially in both groups.

at a fast walking speed, and the level of activation will have differed between muscles. It might have been better if a maximal voluntary isometric contraction had been used for each muscle or muscle group, which is an advised, reliable normalization method in healthy individuals (Burden, 2010). However, selective muscle control can be impaired in children with CP (Graham et al., 2016; Tedroff et al., 2006), making it difficult to maximally activate muscles in the isolated contraction of such a calibration trial. Therefore,

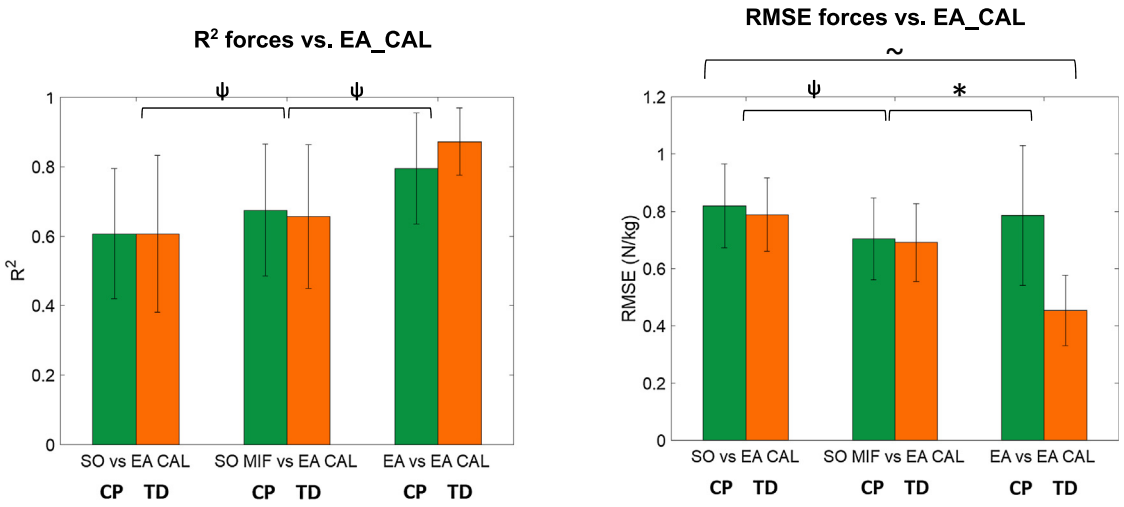

Fig. 5. For each modelling method the agreement with the musculotendon forces estimated by the most personalized model (calibrated EMG-assisted; EA_CAL) was quantified by the R^2 (left) and the RMSE (right). In both groups, switching to an EMG-assisted approach substantially affected the pattern of the musculotendon forces. While in TD children the RMSE was already reduced when using an EMG-assisted approach (EA) instead of static optimization (SO and SO_MIF), in children with CP calibration had a more substantial effect on the estimated forces. ψ indicates a significant main effect between methods; ~ indicates a significant main effect of group; * indicates a significant interaction effect between methods.

it was decided that using gait data was a preferable method for normalization in this study.

A limitation of this study is that in the EMG-assisted approaches only a limited number of muscle activations could be driven by EMG, since only eight EMG measurement were performed per analyzed leg. Activation patterns of the other musculotendon units were checked for abnormalities, however their agreement with experimental EMG data could not be determined. For more extensive assessments of model performance, EMGs from more muscles need to be recorded. In that case, parameters of more musculotendon units of the model could also be calibrated.

Further research should focus on further improving model performance. Advancement of the musculoskeletal model itself is essential to make it more representative. Further personalization of the model is advised, for example by applying imaging techniques such as magnetic resonance imaging and ultrasound to implement subject-specific masses, shapes and sizes of bones, joint mechanisms, and musculotendon units. Implementing neural impairments into the model's control algorithm, such as increased reflexes (Van der Krogt et al., 2016) and synergistic control, might be another step forward in the accuracy of model predictions, especially for children with CP.

This study has shown that EMG-assisted modelling during gait in TD children and children with CP does not significantly penalize the match with net joint moments. Hence, using an EMG-assisted method may contribute to more accurate estimates of musculotendon forces compared to commonly used static optimization methods. This may be especially relevant in children with CP, in which substantial differences in musculotendon forces of some major muscles were found when using a calibrated EMG-assisted approach. It is advised to perform further validation studies, including models with a higher level of personalization, and undertake future research using different EMG-informed approaches.

Declaration of Competing Interest

The authors declare no conflict of interest.

Acknowledgements

The authors would like to thank Marjolein Piening, Eline Flux, Giorgio Davico and the participants and their parents for their support of the project. This project was partially funded by the MD-Paedigree project: A Model-Driven Paediatric European Digital Repository, partially funded by the European Commission under P7-ICT-2011-9 program (600932).

Appendix A. Supplementary material

Supplementary data to this article can be found online at https://doi.org/10.1016/j.jbiomech.2019.05.026.

References

Buchanan, T.S., Lloyd, D.G., 1995. Muscle activity is different for humans performing static tasks which require force control and position control. Neurosci. Lett. 194, 61–64.
Buchanan, T.S., Shreeve, D.A., 1996. An evaluation of optimization techniques for the prediction of muscle activation patterns during isometric tasks. J. Biomech. Eng. 118, 565–574.
Burden, A., 2010. How should we normalize electromyograms obtained from healthy participants? What we have learned from over 25years of research. J. Electromyogr. Kinesiol. 20, 1023–1035.
Cans, C., 2000. Surveillance of cerebral palsy in Europe: a collaboration of cerebral palsy surveys and registers. Dev. Med. Child Neurol. 42, 816–824.
Carbone, V., van der Krogt, M.M., Koopman, H.F.J.M., Verdonschot, N., 2016. Sensitivity of subject-specific models to hill muscle-tendon model parameters in simulations of gait. J. Biomech. 49, 1953–1960.
Crowninshield, R.D., Brand, R.A., 1981. A physiologically based criterion of muscle force prediction in locomotion. J. Biomech. 14, 793–801.
Delp, S.L., Anderson, F.C., Arnold, A.S., Loan, P., Habib, A., John, C.T., Guendelman, E., Thelen, D.G., 2007. OpenSim: Open-source software to create and analyze dynamic simulations of movement. IEEE Trans. Biomed. Eng. Eng. 54, 1940–1950.
Delp, S.L., Loan, J.P., Hoy, M.G., Zajac, F.E., Topp, E.L., Rosen, J.M., 1990. An interactive graphics-based model of the lower extremity to study orthopaedic surgical procedures. IEEE Trans. Biomed. Eng.
Farina, D., Negro, F., 2012. Accessing the neural drive to muscle and translation to neurorehabilitation technologies. IEEE Rev. Biomed. Eng. 5, 3–14.
Gerus, P., Sartori, M., Besier, T.F., Fregly, B.J., Delp, S.L., Banks, S.A., Pandy, M.G., D'Lima, D.D., Lloyd, D.G., 2013. Subject-specific knee joint geometry improves predictions of medial tibiofemoral contact forces. J. Biomech. 46, 2778–2786.
Graham, H.K., Rosenbaum, P., Paneth, N., Dan, B., Lin, J.-P., Domiano, D.L., Becher, J. G., Gaebler-Spira, D., Colver, A., Reddihough, D.S., Crompton, K.E., Lieber, R.L., 2016. Cerebral palsy. Nat. Rev. Dis. Prim. 2, 1–24.
Hamner, S.R., Seth, A., Delp, S.L., 2010. Muscle contributions to propulsion and support during running. J. Biomech. 43, 2709–2716.
Hermens, H.J., Freriks, B., Merletti, R., Stegeman, D., Blok, J., Rau, G., Disselhorst-Klug, C., Hägg, G., 1999. European Recommendations for Surface ElectroMyoGraphy, Roessingh Research and Development.
Hoang, H.X., Diamond, L.E., Lloyd, D.G., Pizzolato, C., 2019. A calibrated EMG-informed neuromusculoskeletal model can appropriately account for muscle

co-contraction in the estimation of hip joint contact forces in people with hip osteoarthritis. J. Bioech. 83, 134–142.
Hoang, H.X., Pizzolato, C., Diamond, L.E., Lloyd, D.G., 2018. Subject-specific calibration of neuromuscular parameters enables neuromusculoskeletal models to estimate physiologically plausible hip joint contact forces in healthy adults. J. Biomech. 80, 111–120.
Kainz, H., Goudriaan, M., Falisse, A., Huenaerts, C., Desloovere, K., De Groote, F., Jonkers, I., 2018. The influence of maximum isometric muscle force scaling on estimated muscle forces from musculoskeletal models of children with cerebral palsy. Gait Posture 65, 213–220.
Liu, M.Q., Anderson, F.C., Schwartz, M.H., Delp, S.L., 2008. Muscle contributions to support and progression over a range of walking speeds. J. Biomech. 41, 3243–3252.
Lloyd, D.G., Besier, T.F., 2003. An EMG-driven musculoskeletal model to estimate muscle forces and knee joint moments in vivo. J. Biomech. 36, 765–776.
Lloyd, D.G., Buchanan, T.S., 2001. Strategies of muscular support of varus and valgus isometric loads at the human knee. J. Biomech. 34, 1257–1267.
Michnik, R., Jurkojć, J., Pauk, J., 2009. Identification of muscles forces during gait of children with foot disabilities. Mechanika 6, 48–51.
Milner, T.E., Cloutier, C., 1998. Damping of the wrist joint during voluntary movement. Exp. Brain Res. 122, 309–317.
Modenese, L., Phillips, A.T.M., Bull, A.M.J., 2011. An open source lower limb model: Hip joint validation. J. Biomech. 44, 2185–2193.
Out, L., Vrijkotte, T.G.M., van Soest, A.J., Bobbert, M.F., 1996. Influence of the parameters of a human triceps surae muscle model on the isometric torque-angle relationship. J. Biomech. Eng. 118, 17–25.
Palisano, R., Rosenbaum, P., Walter, S., Russell, D., Wood, E., Galuppi, B., 1997. Development and reliability of a system to classify gross motor function in children with cerebral palsy. Dev. Med. Child Neurol. 39, 214–223.
Pizzolato, C., Lloyd, D.G., Sartori, M., Ceseracciu, E., Besier, T.F., Fregly, B.J., Reggiani, M., 2015. moments during dynamic motor tasks. J. Biomech. 48, 3929–3936.
Sartori, M., Farina, D., Lloyd, D.G., 2014. Hybrid neuromusculoskeletal modeling to best track joint moments using a balance between muscle excitations derived from electromyograms and optimization. J. Biomech. 47, 3613–3621.
Sartori, M., Reggiani, M., Farina, D., Lloyd, D.G., 2012. EMG-driven forward-dynamic estimation of muscle force and joint moment about multiple degrees of freedom in the human lower extremity. PLoS One 7. e52618.
Scovil, C.Y., Ronsky, J.L., 2006. Sensitivity of a Hill-based muscle model to perturbations in model parameters. J. Biomech. 39, 2055–2063.
Serrancolí, G., Kinney, A.L., Fregly, B.J., Font-Llagunes, J.M., 2016. Neuromusculoskeletal model calibration significantly affects predicted knee contact forces for walking. J. Biomech. Eng. 138. 081001.
Steele, K.M., DeMers, M.S., Schwartz, M.S., Delp, S.L., 2012. Compressive tibiofemoral force during crouch gait. Gait Posture 35, 556–560.
Steele, K.M., Seth, A., Hicks, J.L., Schwartz, M.S., Delp, S.L., 2010. Muscle contributions to support and progression during single-limb stance in crouch gait. J. Biomech. 43, 2099–2105.
Tax, A.A.M., Denier van der Gon, J.J., Erkelens, C.J., 1990. Differences in coordination of elbow flexor muscles in force tasks and in movement tasks. Exp. Brain Res. 81, 567–572.
Tedroff, K., Knutson, L.M., Soderberg, G.L., 2006. Synergistic muscle activation during maximum voluntary contractions in children with and without spastic cerebral palsy. Dev. Med. Child Neurol. 48, 789.
Thelen, D.G., 2003. Adjustment of muscle mechanics model parameters to simulate dynamic contractions in older adults. J. Biomech. Eng. 125, 70.
Thelen, D.G., Anderson, F.C., 2006. Using computed muscle control to generate forward dynamic simulations of human walking from experimental data. J. Biomech. 39, 1107–1115.
Thelen, D.G., Anderson, F.C., Delp, S.L., 2003. Generating dynamic simulations of movement using computed muscle control. J. Biomech. 36, 321–328.
Trinler, U., Leboeuf, F., Hollands, K., Jones, R., Baker, R., 2018. Estimation of muscle activation during different walking speeds with two mathematical approaches compared to surface EMG. Gait Posture 64, 266–273.
Van der Krogt, M.M., Bar-On, L., Kindt, T., Desloovere, K., Harlaar, J., 2016. Neuro-musculoskeletal simulation of instrumented contracture and spasticity assessment in children with cerebral palsy. J. Neuroeng. Rehabil., 13
Van der Krogt, M.M., Delp, S.L., Schwartz, M.H., 2012. How robust is human gait to muscle weakness? Gait Posture 36, 113–119.
Wesseling, M., De Groote, F., Meyer, C., Corten, K., Simon, J.-P., Desloovere, K., Jonkers, I., 2016. Subject-specific musculoskeletal modelling in patients before and after total hip arthroplasty. Comput. Methods Biomech. Biomed. Engin. 19, 1683–1691.
Xiao, M., Higginson, J., 2010. Sensitivity of estimated muscle force in forward simulation of normal walking. J. Appl. Biomech. 26, 142–149.